Dissipative structures induced by spin-transfer torques in nanopillars

Alejandro O. León* and Marcel G. Clerc†
Departamento de Física, Facultad de Ciencias Físicas y Matemáticas, Universidad de Chile, Casilla 487-3, Santiago, Chile

Saliya Coulibaly‡
Laboratoire de Physique des Lasers, Atomes et Molécules, CNRS UMR 8523, Université des Sciences et Technologies de Lille - 59655 Villeneuve d'Ascq Cedex, France

(Received 8 November 2013; published 10 February 2014)

Macroscopic magnetic systems subjected to external forcing exhibit complex spatiotemporal behaviors as result of dissipative self-organization. Pattern formation from a uniform magnetization state, induced by the combination of a spin-polarized current and an external magnetic field, is studied for spin-transfer nano-oscillator devices. The system is described in the continuous limit by the Landau-Lifshitz-Gilbert equation. The bifurcation diagram of the quintessence parallel state, as a function of the external field and current, is elucidated. We have shown analytically that this state exhibits a spatial supercritical quintic bifurcation, which generates in two spatial dimensions a family of stationary stripes, squares, and superlattice states. Analytically, we have characterized their respective stabilities and bifurcations, which are controlled by a single dimensionless parameter. This scenario is confirmed numerically.

DOI: 10.1103/PhysRevE.89.022908 PACS number(s): 05.45.Yv, 89.75.Kd

I. INTRODUCTION

Macroscopic systems maintained out of equilibrium, under the influence of injection and dissipation of energy and momenta, are characterized by exhibiting self-structuring phenomena [1–5]. In the course of the last decades, much effort has been devoted to the study of pattern formation or dissipative structures arising in diverse branches of natural sciences (see the textbooks [4–7] and the references therein). These patterns are the result of the interplay between the linear gain and the nonlinear saturation mechanisms. In many physical systems, these structures emerge as a spatial instability of a uniform state when a control parameter is changed and surpasses a critical value, which usually corresponds to an imbalance of forces. Thus, these bifurcations correspond to spontaneous symmetry breaking [3,8]. Near the instability there is a separation of time scales between the evolution of critical and slave spatial modes, whose amplitudes grow or decrease exponentially, respectively. This separation of scales reduces the dynamics into a few spatial modes, which lead the behavior of the system under study (see [1–4,8–10]). Close to the spatial instability, a unified description of pattern formation can be achieved with the method of amplitude equations.

In one-dimensional extended systems, the dynamics at the onset of bifurcation are generally described by a complex amplitude. The magnitude of the amplitude, at equilibrium, satisfies a power law as a function of the bifurcation parameter [11].

The above scenario changes drastically in two spatial dimensions as result of spatial isotropy. A large number of critical modes can be activated, which correspond to the stripe patterns with different orientations, initially creating several domains separated by local and extended defects. Later on, domains and defects evolve until they reach an equilibrium state [2,2–5]. Near the bifurcation, these equilibria are formed by combinations of a few spatial modes, such as stripes, squares, and hexagons [3,4,8]. Far from the spatial bifurcation, the equilibria observed are more elaborate structures such as quasipatterns [12,13], superlattices [8], and labyrinths [14]. All these stationary states are composed by a large number of modes. The fundamental tools for the understanding of these states are the theory of groups, defects interactions, and amplitude equations.

The control of magnetization in ferromagnetic nanopillars has been the subject of intensive study in recent years [15–17] for its technological applications, such as magnetic sensors, magnetic read heads, data memory, magnetic switching, and spin transistors. In such devices, an electric current J applied through the spin-valve transfers spin angular momentum to a ferromagnetic layer from another film with fixed magnetization. This effect is known as the spin-transfer torque [18–22]. When the direct current overcomes a critical value, spin-transfer torque switches the magnetization and/or carries it into a stable precession in the radio-frequency domain. Recently, it has been shown that large precessional magnetic motions can be destabilized by patternlike perturbations in nanopillars [23]. Figure 1(a) represents schematically a spin-valve structure composed by two magnetic layers (dark layers), the free and the fixed one, separated by a metallic nonmagnetic spacer (light layers).

Most of previous research has focused on the study of uniform magnetization dynamics. This approach is known as the macrospin approximation [21]. A natural question that arises is whether the spin-transfer process is capable of generating self-organized stationary structures from an homogeneous current. This phase transition can become important because it generates nonuniform stationary configurations for parameter values where the parallel state was predicted to be stable by the macrospin model.

The aim of this manuscript is to characterize the formation of patterns from a uniform magnetization state in one and two spatial dimensions in spin-transfer nano-oscillators induced

*aoleon@dfi.uchile.cl
†marcel@dfi.uchile.cl
‡saliya.coulibaly@univ-lille1.fr

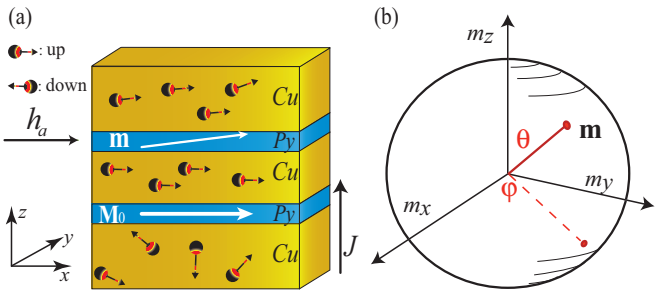

FIG. 1. (Color online) Nanopillar device. (a) Schematic representation of the spin-transfer torque nano-oscillator setup. The dark (blue) and light (yellow) layers represent magnetic and nonmagnetic metal films, respectively. Electrons are depicted schematically with their respective spins. J and h_a are the electric current through the spin valve and the external magnetic field, both effects are parallel to the easy axes of the ferromagnetic layer under study. $\mathbf{M}_o$ stands for the magnetization of the fixed layer. (b) Spherical representation of the magnetization $\mathbf{m}$.

by the combination of a spin-polarized current and an external magnetic field.

The system is described in the continuous limit by the Landau-Lifshitz-Gilbert equation with a spin-transfer torque term. Through a linear analysis we characterize entirely the bifurcation diagram of the parallel state submitted to an external magnetic field. Based on amplitude equations we show that the system has a quintic supercritical bifurcation. In two spatial dimensions, we observe the emergence of stripes or superlattices at the onset of the bifurcation. Analytically, we characterize the respective bifurcation diagram, which is controlled by a single parameter. This scenario is qualitatively and quantitatively verified numerically.

The manuscript is organized as follows. In Sec. II, the dynamics of the free magnetic layer in the spin-valve with spin-polarized current are described theoretically. The bifurcation diagram of the one-dimensional configuration is studied in Sec. III. The spatial bifurcation exhibited by the system is characterized by means of amplitude equations. The patterns in the two-dimensional configuration are studied in Sec. IV. The dynamics of four-modes and their conjugates are analyzed in detail. Our conclusions and remarks are left to the final section.

II. SPIN VALVE WITH SPIN-TRANSFER TORQUE

Let us consider a nanopillar device with pinned layer magnetization along the positive x axis as depicted by Fig. 1(a). The energy E of the free magnetic layer has the form [24]

$$E = \tfrac{1}{2}\mu_0 M_s^2(\nabla\mathbf{m})^2 + \tfrac{1}{2}\mu_0 M_s^2\beta_z(\mathbf{m}\cdot\hat{\mathbf{z}})^2 - \tfrac{1}{2}\mu_0 M_s^2\beta_x(\mathbf{m}\cdot\hat{\mathbf{x}})^2 - \mu_0 M_s^2\mathbf{m}\cdot\mathbf{h_a}, \quad (1)$$

where $\mathbf{M}(\mathbf{r},t)$ is the magnetization in the free magnetic layer and $\{\mathbf{r},t\}$ stand for the spatial and temporal coordinates, respectively. $\mathbf{m}(\mathbf{r},t) = \mathbf{M}/M_s$ is the unitary magnetization vector, M_S is the saturation magnetization. β_x and β_z are combinations of the normalized anisotropy and demagnetization constants with respect to the appropriate axes, where β_x (β_z) favors (disfavors) the free magnetization in the x axis (z axis). $\mu_0 M_s^2/2$ is the shape anisotropy energy of the thin film, and $\mathbf{h_a} = h_a\hat{x}$ is the external magnetic field that we set to point along the x axis [see Fig. 1(a)]. The gradient operator is $\nabla \equiv \hat{\mathbf{x}}\partial_X + \hat{\mathbf{y}}\partial_Y + \hat{\mathbf{z}}\partial_Z$ and distances are nondimensionalized with respect to the exchange length $l_{\rm ex} \equiv \sqrt{2A/(\mu_0 M_s^2)}$ where A is the exchange coupling in the ferromagnet.

The dynamics of the magnetization of this free layer can then be described by the Landau-Lifshitz-Gilbert equation (LLG) under the influence of a spin-transfer torque term [25]

$$\frac{\partial\mathbf{m}}{\partial t} = \frac{\gamma}{M_s}\mathbf{m}\times\frac{\delta E}{\delta\mathbf{m}} + g\ \mathbf{m}\times(\mathbf{m}\times\hat{\mathbf{x}}) + \alpha\mathbf{m}\times\frac{\partial\mathbf{m}}{\partial t}, \quad (2)$$

with

$$\frac{\delta E}{\delta\mathbf{m}} = -\frac{1}{2}\mu_0 M_s^2[(h_a+\beta_x m_x)\hat{x} - \beta_z m_z\hat{z} + \nabla^2\mathbf{m}], \quad (3)$$

and γ is the gyromagnetic ratio. The spin-transfer torque coefficient is defined by $g \equiv \mathcal{P}(\hbar/2)(J/d|e|)f(\mathbf{m}\cdot\hat{\mathbf{x}})$, where $\mathcal{P}$ describes the electron polarization at the interface between the magnet and the spacer, J the current density, d the thickness of the layer, and e the electric charge. The parameter g is negative when the electrons flow from the fixed to the free layer. The first term of the right-hand side of Eq. (2) accounts for precessions, the second one gives account of the spin-transfer effect and the last one is the Gilbert damping, which accounts for dissipation of the energy. The parameter α rules the intensity of the damping. We note that in the present analysis the nonlocal effects of demagnetization fields have been approximated by a renormalization of the anisotropy coefficients. This simplifies drastically the equations, allowing us to have access to analytical calculations. Moreover, we have considered this approach because it is a good approximation for thin film systems with dimensions in the nanometer range [26] and also in the case where the magnetization has small deformations with respect to the uniform state [24].

The dynamics of LLG are characterized by the conservation of the magnitude of magnetization $\|\mathbf{m}\|$, since $\mathbf{m}$ and $\partial_t\mathbf{m}$ are perpendicular. Hence, the dynamics of Eq. (2) consist of rotations of $\mathbf{m}$. The LLG model, Eq. (2), admits two natural steady and uniform states: $\mathbf{m} = \pm\hat{x}$, which represent a free magnetization that is parallel (+) or antiparallel (−) to the fixed magnetization $\mathbf{M}_0$ [see Fig. 1(a)]. Both states correspond to extrema of energy Eq. (1). Hereafter, for the sake of simplicity, we will consider the following scaling and dimensioning of units $\mu_0 M_s^2/2 = 1$, $\gamma/M_s = 1$ and $\|\mathbf{m}\| = 1$ without loss of generality.

The specific form of the angular dependence of spin-transfer function $f(\mathbf{m}\cdot\hat{x})$ is sensitive to all the spin-transport parameters and much theoretical effort has been involved in establishing its relation with microscopic properties [18,27–30]. For the sake of simplicity, we consider the case $f \simeq 1$, which is valid for certain types of nanopillars [31,32].

A. Spherical representation of LLG model

Due to the conservation of the magnitude of the free magnetization, the numerical integration of Eq. (2) in the Cartesian representation for the magnetization can be a nontrivial task. Let us introduce the following spherical representation of the free magnetization

$$\mathbf{m} = \sin\theta(\cos\varphi\hat{x} + \sin\varphi\hat{y}) + \cos\theta\hat{z}, \quad (4)$$

where the angles are outlined in Fig. 1(b) and the north pole lies on the m_z axis. Introducing the previous representation in Eq. (2), one obtains the following set of equations

$$\begin{aligned}\partial_\tau\theta &= \sin\theta\nabla^2\varphi + 2\cos\theta\nabla\varphi\cdot\nabla\theta + \alpha\nabla^2\theta \\ &\quad - \frac{\alpha}{2}\sin 2\theta(\nabla\varphi)^2 - (h_a+\alpha g)\sin\varphi \\ &\quad - \frac{\beta_x}{2}\sin\theta\sin 2\varphi + (\alpha h_a - g)\cos\varphi\cos\theta \\ &\quad + \frac{\alpha}{2}\sin 2\theta[\beta_z + \beta_x\cos^2\varphi], \\ \sin\theta\partial_\tau\varphi &= \alpha\sin\theta\nabla^2\varphi + 2\alpha\cos\theta\nabla\varphi\cdot\nabla\theta - \nabla^2\theta \\ &\quad + \frac{1}{2}\sin 2\theta(\nabla\varphi)^2 + (g-\alpha h_a)\sin\varphi \\ &\quad - \alpha\frac{\beta_x}{2}\sin\theta\sin 2\varphi - (\alpha g + h_a)\cos\varphi\cos\theta \\ &\quad - \frac{1}{2}\sin 2\theta[\beta_z + \beta_x\cos^2\varphi], \end{aligned} \tag{5}$$

where $\tau = t/(1+\alpha^2)$. To complement the theoretical study of the dynamics exhibited by the nanopillar, we have conducted numerical simulations with the spherical representation of Eq. (5) in order to preserve the magnitude of the magnetization. In all numerical simulations performed throughout this work, the space is discretized with finite differences where spatial differential operators are approximated with centered schemes of order 6. The magnetization for each element of the grid is obtained by solving Eq. (5) by means of a fourth-order Runge-Kutta algorithm. With this discretization, each volume of the layer interacts with twelve of its neighbors through the ferromagnetic exchange torque. Notice that the nonlocal demagnetization is not a mechanism of spatial coupling, because it has been approximated by the hard-axis anisotropy term proportional to β_z in Eq. (1).

Numerical simulations have also been conducted with stereographic representation [33], an alternative method that guarantees the preservation of the magnitude of **m**. The results provided by both representations are equal. Both Periodic and Neumann boundary conditions are used.

III. ONE-DIMENSIONAL NANOPILLAR

The parallel state, $\mathbf{m} \equiv \mathbf{m_p} = \hat{x}$, is a trivial steady state of LLG equation. Since the external magnetic field is parallel to the easy axis, $\mathbf{h}_a = h_a\hat{x}$, $h_a > 0$ will produce a torque that favors the parallel configuration. On the other hand, fields pointing against $\hat{x}$ will stabilize the antiparallel state. For near-parallel configurations, electric current flowing from the fixed to the free layer, $g < 0$, will contribute to the stabilization of the parallel state. Therefore, the self-organization dynamics appears as a balance between two opposite effects: the current stabilizing the parallel state and the external field destabilizing it. In this section, we analyze the bifurcation diagram of the parallel state in the one-dimensional configuration.

A. Linear stability analysis of parallel state

The parallel state in the spherical representation takes the form $(\theta,\varphi) = (\pi/2, 0)$. To study the dynamics around the parallel state we consider a perturbated state of the form

$$\begin{pmatrix}\theta(x,t)\\ \varphi(x,t)\end{pmatrix} = \begin{pmatrix}\pi/2\\ 0\end{pmatrix} + \begin{pmatrix}\delta\theta_k(t)\\ \delta\varphi_k(t)\end{pmatrix}e^{ikx} + \text{c.c.},$$

where the small amplitudes $\{\delta\theta_k(t), \delta\varphi_k(t)\}$ account for Fourier modes and the symbol c.c. represents the complex conjugate. Considering the above perturbation in Eq. (5) at linear order, we obtain

$$\frac{d}{dt}\begin{pmatrix}\delta\theta_k\\ \delta\varphi_k\end{pmatrix} = \begin{bmatrix} g-\alpha a & -(a-\beta_z+\alpha g)\\ a+\alpha g & g-\alpha(a-\beta_z)\end{bmatrix}\begin{pmatrix}\delta\theta_k\\ \delta\varphi_k\end{pmatrix}, \tag{6}$$

with $a \equiv h_a + \beta_x + \beta_z + k^2$. Introducing an eigenmode ansatz $\delta\theta_k(t) = \delta\theta_k e^{\lambda t}$ and $\delta\varphi_k(t) = \delta\varphi_k e^{\lambda t}$, we find the following characteristic polynomial

$$\lambda^2 + b\lambda + c = 0, \tag{7}$$

where

$$b \equiv \alpha(2a-\beta_z) - 2g,$$
$$c \equiv (g-\alpha a)(g-\alpha(a-\beta_z)) + (a+\alpha g)(a+\alpha g-\beta_z).$$

For simplicity we study first the parameter region where the inhomogeneous perturbations decay and the bifurcating mode is homogeneous ($k = 0$). If $b = 0$ and $c > 0$, then the system exhibits an Andronov-Hopf bifurcation [34]. In the space of parameters $\{g, h_a\}$ the Andronov-Hopf instability curve is represented by the tilted straight line (see Fig. 2). Then, the parallel state becomes unstable through an oscillatory precession with frequency $\sqrt{c}$. This type of dynamics has

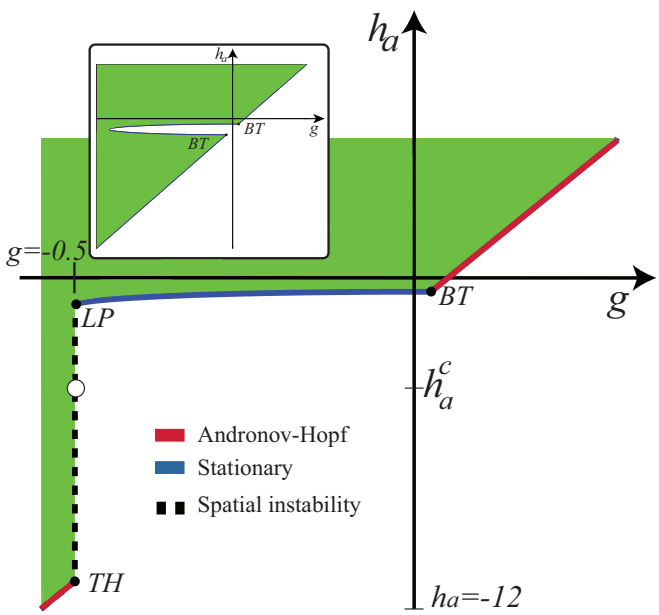

FIG. 2. (Color online) Bifurcation diagram of parallel state in the parameters space $\{g, h_a\}$. The parallel state is stable in the dark region. The thick diagonal line accounts for the Andronov-Hopf bifurcation. The horizontal curve realizes stationary instability. $\{BT, LP, TH\}$ represent the codimension two points associated to Bogdanov-Takens, Lifshitz-point, and Turing-Hopf instabilities, respectively. The vertical dashed line accounts for the spatial instability curve. The inset represents the bifurcation diagram in the case where spatial effects are ignored.

been reported on a nanopillar, where the frequency is typically of the order of the microwave [20].

In the case where the parameter c vanishes and $b \neq 0$, the system exhibits a stationary bifurcation for the parallel state [34]. This instability is characterized by a curve in the $\{g,h_a\}$ plane (see the inset in Fig. 2). In this region of the parameters space, the parallel state becomes unstable and eventually saturates into other states. Simultaneous confluence of a stationary instability and Andronov-Hopf bifurcation is a codimension two point, usually called Bogdanov-Takens [35]. This instability is characterized by two eigenvalues simultaneously crossing the origin of the complex plane with a single associated eigenvector. At this point we have $b = c = 0$. This point in the $\{g,h_a\}$ plane is denoted BT in Fig. 2. In other terms, since we have ignored the spatial dependences, the system exhibits two Bogdanov-Takens points as illustrated in the inset of Fig. 2. It is important to note that the experimental report made in Ref. [20] is performed around the Bogdanov-Takens point. In addition, this bifurcation diagram clearly emphasizes that when both the magnetic field and the spin-polarized current are positive, they favor and disfavor the parallel state $\mathbf{m_p}$.

The above scenario changes drastically when spatial effects are considered, $k \neq 0$, i.e., when one considers the exchange processes. The eigenvalues will become a function of wave number, $\lambda(k)$. The typical curve of the growth rate as a function of wave number [$\mathrm{Re}(\lambda(k))$] and the dispersion relation [$\mathrm{Im}(\lambda(k))$] are illustrated in Fig. 3(a). Note that the maximum $\mathrm{Re}(\lambda)$ has no-null wave number (k_c). Then changing the parameters of the system, it can exhibit a spatial instability, which analytically corresponds to impose the condition [3]

$$\left.\frac{\partial\lambda}{\partial k}\right|_{k=k_c} = 0, \quad \left.\frac{\partial^2\lambda}{\partial^2 k}\right|_{k=k_c} < 0, \quad \text{and} \quad \lambda(k_c) = 0.$$

The first relation determines the critical wave number and the other the respective condition of instability. Applying the above conditions, we find the following length and critical condition

$$k_c^2 = -h_a - \left(\beta_x + \frac{\beta_z}{2}\right), \qquad g_c = -\frac{\beta_z}{2}. \tag{8}$$

Since $k_c^2 \geqslant 0$, the external field must point against the parallel equilibrium for this bifurcation. The expression above corresponds to a vertical segment on the $\{g,h_a\}$ plane, which is represented by the dashed line of Fig. 2. In that zone, the external field h_a destabilizes the parallel state and $g < 0$ favors it through the current transport the magnetic moment from the fixed layer. The instability occurs when the current is not strong enough to balance with the external field and maintain the magnetization parallel. The emergence of a spatial instability with a divergent wavelength is generated from a Lifshitz point [3,36]. This critical point is characterized by the confluence of stationary instability and a spatial bifurcation. This is a codimension three point introduced for phase transitions in helicoidal ferromagnetic states [36]. Figure 2 represents this point with the symbol LP. Analogously spatial instability may coincide with the Andronov-Hopf bifurcation at a point of codimension two, which is usually denominated Turing-Hopf point [37,38]. Around this point the system is characterized by the emergence of waves. Figure 2 depicts this point by the symbol TH.

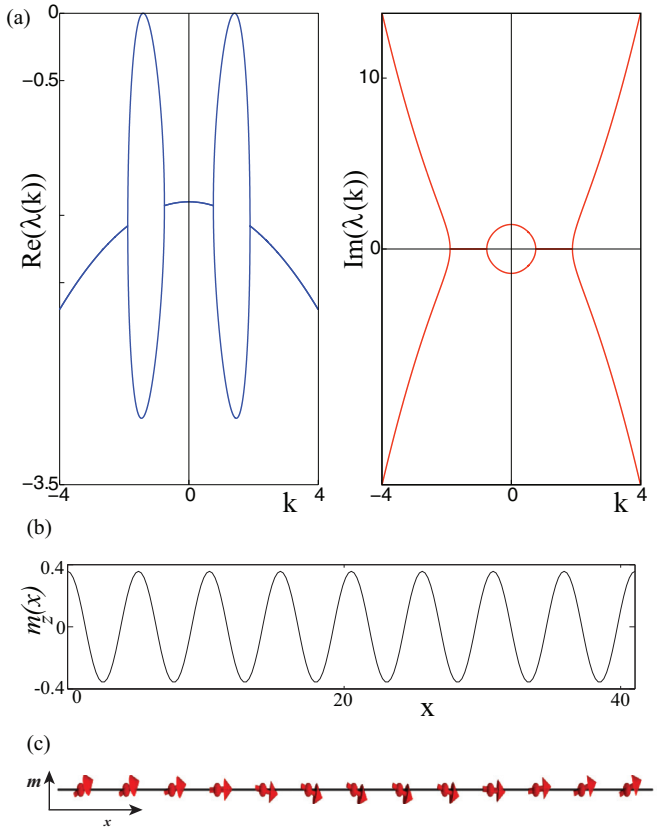

FIG. 3. (Color online) (a) Growth rate as a function of wave number [$\mathrm{Re}(\lambda(k))$] and the dispersion relation [$\mathrm{Im}(\lambda(k))$]. (b) $m_z(x)$ for the parameter values $g = -0.4976, h_a = -2.5, \beta_x = 0.5, \beta_z = 1$, $\alpha = 0.05$. The size of the box is chosen to admit 8 wavelengths. (c) Spin representation of one wavelength of the above state.

In physical units, the wavelength is $\Lambda = 2\pi l_{ex}/\sqrt{|h_a| - \beta_x - \beta_z/2}$. Notice that the parameter h_a permits the wavelength to vary between the the size of the device and the exchange length l_{ex}, in this last situation the continuous description becomes questionable.

When one crosses the dashed vertical line, the parallel state $\mathbf{m_p}$ becomes unstable giving rise to the appearance of a spatial pattern. Figure 3(b) shows an example of the observed stationary pattern. In order to understand this pattern analytically in Sec. III B we will carry out a weakly nonlinear analysis close to the spatial instability. This nonlinear analysis is based on the amplitude equations method [9].

B. Weakly nonlinear analysis

To characterize the dynamics of the pattern close to the spatial instability, we consider the following approximation for the free magnetization

$$\begin{pmatrix}\theta\\ \varphi\end{pmatrix} \approx \begin{pmatrix}\pi/2\\ 0\end{pmatrix} + [T(x,t)e^{ik_c x} + \bar{T}(x,t)e^{-ik_c x}]\begin{pmatrix}1\\ 1\end{pmatrix}, \tag{9}$$

where $\epsilon \equiv g - g_c$ is the bifurcation parameter. $T(x,t)$ describes the slowly varying amplitude of the critical spatial mode $\mathbf{m_c}(x)$, which corresponds in a Cartesian representation to the vector

$$\mathbf{m_c} = \begin{pmatrix} 1 \\ T(x,t)e^{ik_c x} + \bar{T}(x,t)e^{-ik_c x} \\ -T(x,t)e^{ik_c x} - \bar{T}(x,t)e^{-ik_c x} \end{pmatrix}, \tag{10}$$

$\bar{T}$ stands for the complex conjugate of T, and h.o.t. accounts for the higher-order corrections. Introducing the above ansatz Eq. (9) in Eq. (5), and imposing a solvability condition after calculations we obtain (quintic real Ginzburg-Landau equation)

$$\partial_t T = \epsilon T - \frac{\left(6\beta_x + 3\beta_z - 2k_c^2\right)^2}{4\beta_z} T|T|^4 + \frac{4k_c^2}{\beta_z}\partial_{xx} T. \tag{11}$$

To obtain this equation we have considered the following scaling $T \sim \epsilon^{1/4}$, $\partial_t \sim \epsilon$, and $\partial_x \sim \epsilon^{1/2}$. Then, this amplitude equation is of order $\epsilon^{5/4}$ and the corrections are of order $\epsilon^{7/4}$. Then the characteristic time scale of patterns will be ϵ^{-1}, or, in physical units of $[\gamma M_s(g - g_c)]^{-1}$. Equation (12) has uniform solutions of the form

$$T(x,t) = \left[4\beta_z \frac{(g - g_c)}{\left(6\beta_x + 3\beta_z - 2k_c^2\right)^2}\right]^{1/4}, \tag{12}$$

which represents the pattern amplitude as a function of the physical parameters. Note that this amplitude increases with 1/4 power of the bifurcation parameter, $|T| \sim \epsilon^{1/4}$. Numerically from the LLG equation Eq. (5), we have verified this prediction. Indeed, we have represented in Fig. 4 the amplitude of the pattern (dotted) and formula Eq. (12). As can be seen from this figure, the two results are in good agreement. Far from the threshold the numerical and analytical results start to disagree. The higher-order terms are responsible for this difference.

Generically, the amplitude of the patterns near the spatial bifurcation follows a power law of the square root type [3,11], due to the cubic nonlinearity. However, in the nanopillar oscillator the pattern is controlled by the quintic nonlinearity. Although supercritical quintic bifurcations are less common than supercritical cubic instabilities in the context of parametric instabilities such bifurcations are generic [39,40] and even this has been reported experimentally [41].

Note that the coefficient of the quintic term is modified with the external magnetic field, h_a through its dependence on k_c (cf. Eqs. 8). There is a critical value of the external magnetic field,

$$h_a^c = -4\left(\beta_x + \frac{\beta_z}{2}\right), \tag{13}$$

for which the quintic coefficient vanishes. The dynamics around this point is led by the seventh nonlinearity in the amplitude equation. Notwithstanding, the quintic coefficient always is semidefined positives, that is the spatial instability is always supercritical.

Notice that the parallel state is related with antiparallel one through the transformation $(g, h_a, \varphi) \to (-g, -h_a, \varphi + \pi)$. Therefore, the antiparallel state of the free magnetization has a analogous phase diagram to the parallel state with the opposite sign of the external magnetic field and spin-polarized current.

IV. DYNAMICS IN TWO DIMENSIONS: STRIPES AND SUPERLATTICES

Let us consider a spatial transversal extension of the nanopillar in two dimensions, then the magnetization becomes a field defined in the xy plane, $\mathbf{m}(x,y,t)$. The stability analysis presented in Sec. III remains valid, where the only instability that is modified is the spatial one, due to the presence of an infinite number of critical spatial modes with wave number $|\mathbf{k}| = k_c$. Figures 5 and 7 show the typical pattern observed at the onset of the spatial bifurcation. Unexpectedly, the observed pattern near the bifurcation reveals a greater spatial complexity in comparison to those usually reported at the onset of the spatial instability such as stripes, squares, and hexagons patterns [1–5]. Figure 5 illustrates the number of coupled

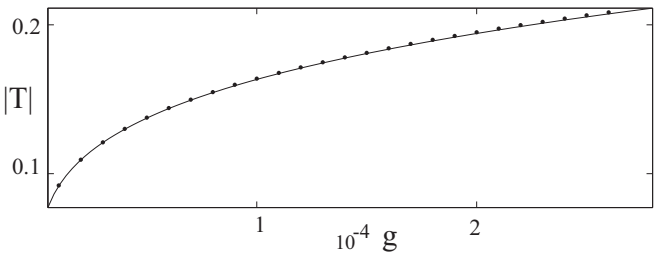

FIG. 4. Pattern amplitude as a function of the spin-polarized current. Points are obtained by numerical simulations of the LLG model for $h_a = -2.5$, $\beta_x = 0.5$, $\beta_z = 1$, and $\alpha = 0.05$. The total length of the simulation box is chosen to admit 8 critical wavelengths. The dotted curve is a fit with a power law where the exponent found is 0.25.

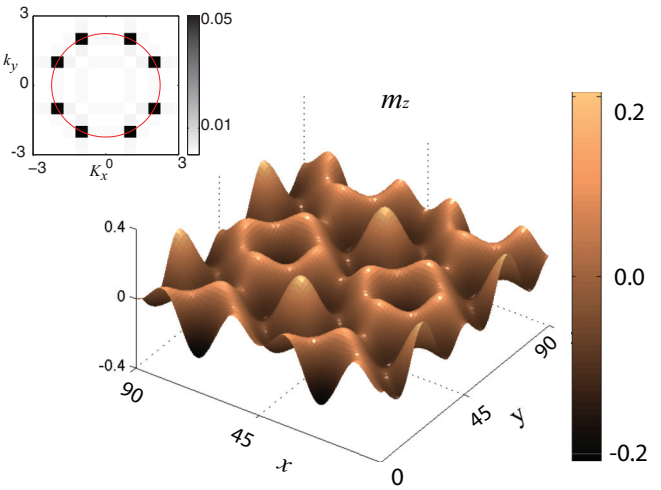

FIG. 5. (Color online) The component m_z of the magnetization in a 90×90 grid, it was obtained by numerical simulations of the LLG model for $g = -0.4999$, $h_a = -6$, $\beta_x = 0.5$, $\beta_z = 1$, and $\alpha = 0.05$. The space is divided into squares of lateral dimension $dx = 0.141\,195$. The inset shows the Fourier transform of m_z, and the circumference shows the critical wavelength k_c.

modes, which corresponds to four spatial modes and their respective conjugate modes. These types of patterns are usually denominated as superlattices [8]. In order to understand the emergence of these patterns analogously to the study that we have conducted on one spatial dimension, we will carry out a weakly nonlinear analysis.

A. Amplitude equations

In two spatial dimensions, the linear stability analysis is similar to those presented in Sec. III. The perturbation of the parallel state reads

$$\begin{pmatrix}\theta(\mathbf{r},t)\\ \varphi(\mathbf{r},t)\end{pmatrix}=\begin{pmatrix}\pi/2\\ 0\end{pmatrix}+\begin{pmatrix}\delta\theta_k(t)\\ \delta\varphi_k(t)\end{pmatrix}e^{i\mathbf{k}\cdot\mathbf{r}}+\text{c.c.},$$

where $\mathbf{r}=(x,y)$ stands for the transverse coordinates of the free magnetic layer. Then we obtain the same characteristic polynomial (7) where k is replaced by $|\mathbf{k}|$. Imposing the conditions of spatial instability we obtain

$$|\mathbf{k}_c|^2=-h_a-\left(\beta_x+\frac{\beta_z}{2}\right),\quad g_c=-\frac{\beta_z}{2}. \tag{14}$$

Therefore, all spatial modes having the same magnitude $|k_c|$ are critical modes.

To study the dynamics of these critical modes we have considered the following ansatz

$$\begin{pmatrix}\theta\\ \varphi\end{pmatrix}=\begin{pmatrix}\pi/2\\ 0\end{pmatrix}+R\sum_{j=1}^{N}A_j(\mathbf{r},\epsilon t)e^{i\mathbf{k}_c^j\cdot\mathbf{r}}\begin{pmatrix}1\\ 1\end{pmatrix}+\text{c.c.}+\text{h.o.t.}, \tag{15}$$

where A_j accounts for the amplitude of the critical spatial mode $\mathbf{k}_c^j$, which we assume is a slow variable in space and time, and N stands for the number of critical spatial modes. Finally, R is a characteristic scale for the amplitude of the patterns given by

$$R=\sqrt[4]{\frac{4\beta_z\epsilon}{(6\beta_x+3\beta_z-2q^2)^2}}. \tag{16}$$

Introducing the above ansatz (15) in Eq. (5), and imposing the condition of solubility after straightforward calculations we obtain the following set of amplitude equations (coupled Newell-Whitehead-Segel equations [2,3,42])

$$\begin{aligned}\partial_t A_j=&A_j-A_j|A_j|^4-\frac{8}{3}\frac{1}{1-D}A_j\sum_{l\neq j}^{N}|A_l|^4\\&+\hat{L}_{nws}(\nabla_j)A_j-\frac{8}{3}\frac{2-3D}{1-D}A_j|A_j|^2\sum_{l\neq j}^{N}|A_l|^2\\&-8A_j\sum_{l\neq j,m\neq j,m\neq l}^{N}|A_l|^2|A_m|^2,\end{aligned} \tag{17}$$

with

$$\hat{L}_{nws}(\nabla_j)\equiv\frac{4}{\beta_z}\left(|k_c|\frac{\partial}{\partial x_{\parallel_j}}-\frac{i}{2}\frac{\partial^2}{\partial x_{\perp_j}^2}\right)^2 \tag{18}$$

is the spatial operator, $\{x_{\parallel_j},x_{\perp_j}\}$ are, respectively, the longitudinal and the transverse coordinates with respect to the vector $\mathbf{k}_c^j$ and

$$D\equiv\frac{2}{3}\frac{q^2}{2\beta_x+\beta_z}=\frac{2|h_a|-2\beta_x-\beta_z}{6\beta_x+3\beta_z}. \tag{19}$$

Note that there is only one parameter, D, which characterizes the dynamics of the system. The above set of equations have derived considering the scaling $|A_j|\sim\epsilon^{1/4}$, $\partial_t\sim\epsilon$, $x_{\parallel}\sim\epsilon^{-1/2}x$, and $x_{\perp_j}\sim\epsilon^{-1/4}x$. Equation (17) accounts for the dynamics of all critical modes. Nevertheless, the size effects discretizing and privilege certain critical modes [8].

B. Size effects in the pattern formation

In the case of considering Neumann boundary conditions, and transverse dimensions L_x and L_y, respectively, the critical spatial modes compatible with the boundary conditions have the form $\mathbf{k}_c^{m,n}=(\pi m/L_x,\pi n/L_y)$ with $\{m,n\}$ integer numbers. Therefore the critical spatial modes must satisfy the relation

$$\pi^2\left(\frac{m^2}{L_x^2}+\frac{n^2}{L_y^2}\right)=|h_a|-\left(\beta_x+\frac{\beta_z}{2}\right). \tag{20}$$

As a result of this discretization—owing to size effects—few couplings between patterns are allowed, such as one mode (stripe pattern), two modes (square pattern), four modes (superlattice pattern), six modes (superlattice pattern), and so forth, and their respective conjugates. Hence, the number of critical modes considered in ansatz (15) are such that $N=1,2,4,6,8,12,\ldots$. Patterns generated by an odd number of critical modes such as hexagons (three modes and their conjugates) are not observed because the system has no quadratic terms [2,3]. These terms are not allowed in the LLG equation due to the symmetries $\varphi\to-\varphi$ and $\theta\to-\theta$.

The relevant question that emerges is: how can we understand the observed equilibria at the onset of the bifurcation? To resolve this question one must study the stability of the stripe state. If this state is unstable then for symmetry reasons the system will display squares or superlattices equilibrium state, consistent with the boundary conditions. In the next section, we will perform the stability analysis of the stripe pattern when one considers few coupled modes and their respective conjugate modes.

C. Bifurcation diagram

To clarify the phase diagram we consider the dynamics of four modes and their complex conjugates ($N=4$) in ansatz (15), and neglecting their spatial coupling, then the amplitude of these modes satisfies

$$\begin{aligned}\partial_t A_1=&A_1-\frac{8}{3}\frac{2-3D}{1-D}A_1|A_1|^2(|A_2|^2+|A_3|^2+|A_4|^2)\\&-A_1(|A_1|^4+8(|A_2|^2|A_3|^2+|A_3|^2|A_4|^2\\&+|A_2|^2|A_4|^2))-\frac{8}{3}\frac{1}{1-D}A_1(|A_2|^4+|A_3|^4+|A_4|^4).\end{aligned} \tag{21}$$

The equations for the other amplitudes are obtained just by interchanging the indexes, for instance, $\partial_t A_2$ is obtained with the replacement $(1,2,3,4) \to (2,1,3,4)$. Notice that the bifurcation diagram is characterized entirely by the line $D \geqslant 0$. This parameter describes the competition between the external magnetic field, anisotropies, exchange, and the critical spin-polarized current. Since the coefficients of the above set of equations are real, then only the magnitudes of the amplitudes are coupled and their respective phases are completely decoupled. Hence, the effective dynamical system that accounts for the pattern formation is of dimension 4.

The above set of equations admits four types of equilibria, one describes the stripe patterns $|A_1| \neq 0$, $A_k = 0$ $(k = \{2,3,4\})$, rhombs $|A_1| = |A_2| \neq 0$, $A_3 = A_4 = 0$, hexagons $|A_1| = |A_2| = |A_3| \neq 0$, $A_4 = 0$, and finally the the superlattice. The superlattice pattern is composed by the four modes $|A_1| = |A_2| = |A_3| = |A_4| = 1$

This superlattice pattern is illustrated in Fig. 5. On the other hand, the stripe patterns correspond to a nonzero amplitude while the other amplitudes are zero, for example $A_1 = 1$, and $A_2 = A_3 = A_4 = 0$. This pattern corresponds to a rolls structure in the $\mathbf{k}_1$ direction.

To study the stability of the stripe pattern, we consider the following perturbation $A_1 = 1 + \chi_1(t)$, $A_2 = \chi_2(t)$, $A_3 = \chi_3(t)$, $A_4 = \chi_4(t)$ $(\chi_i \ll 1)$ and linearizing with respect to the perturbation we get

$$\partial_t \chi_1 = -4\chi_1, \quad \partial_t \chi_2 = -\frac{5+3D}{3(1-D)}\chi_2,$$
$$\partial_t \chi_3 = -\frac{5+3D}{3(1-D)}\chi_3, \quad \partial_t \chi_4 = -\frac{5+3D}{3(1-D)}\chi_4.$$

Then for $D < 1$ $(D > 1)$ the stripe pattern is stable (unstable), and for $D > 1$ the system exhibits stable superlattice patterns. The corresponding bifurcation diagram of the system is shown in Fig. 6. For $D = 1$, the quintic saturation vanishes and higher-order nonlinearities are required. Associated with $D = 1$, the system has an external magnetic field value h_a^c, which is highlighted in Fig. 3.

If one performs the same analysis with $N = 2,6,8,12,\ldots$ modes the stability analysis obtained is exactly the same. Hence, Fig. 6 sketches the bifurcation diagram of the system and Fig. 7 illustrates the observed patterns for $D > 1$. Thus, the region closer to stationary instability—the Lifshitz point—exhibits striped patterns whose saturating mechanism is given by the anisotropies β_x and β_z. In contrast, when $|h_a| > |h_a^c|$

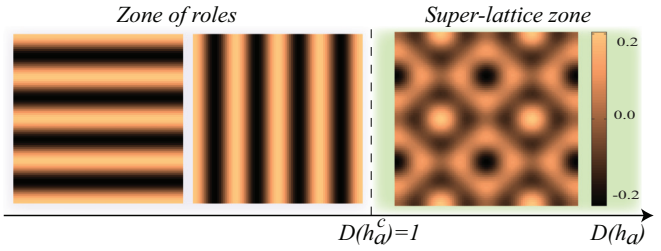

FIG. 6. (Color online) Bifurcation diagram for four-mode models (21). In the left part $(D < 1)$, only rolls are stable. For $D > 1$, the four-modes state is stable. A more general scenario for $D > 1$ is illustrated in Fig. 7.

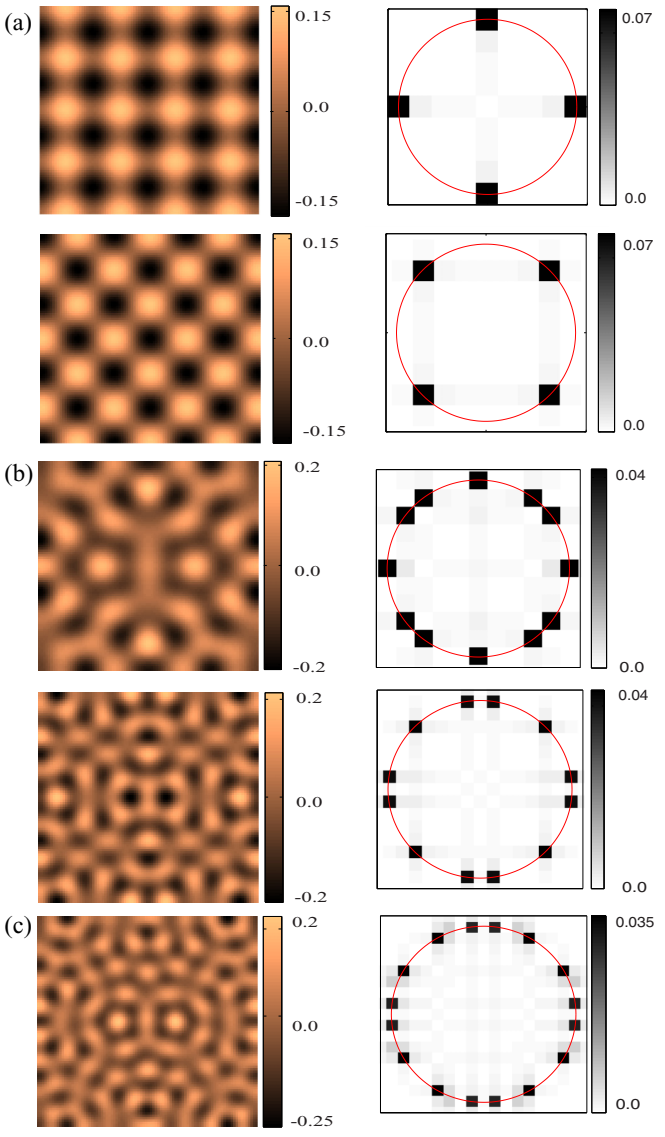

FIG. 7. (Color online) The system size selects the stability of the stationary equilibria for $D > 1$. (a) Squares. The top (down) solution is obtained with $dx = 0.126\,289$ $(dx = 0.133\,949)$. (b) Superhexagons. A $dx = 0.157\,861$ $(dx = 0.223\,25)$ was used for the top (down) state. (c) Eight-mode superlattices, $dx = 0.254\,543$. The other parameters are the same that we considered in Fig. 5.

the system exhibits superlattice patterns. Since large negative magnetic fields penalize configurations near the parallel state, then all admitted modes grow. Pattern solutions obtained for the same parameters that were used on Fig. 5. The exchange free energy term grows as $(\nabla \mathbf{m})^2 \sim q^2|A_j|^2 \sim |h_a||A_j|^2$, then it makes the superlattices saturate. As one continues increasing the bifurcation parameter ϵ, by means of decreasing the modulus of the spin-polarized current g, patterns exhibit complex spatiotemporal behavior. Work in this direction is in progress.

V. CONCLUSIONS AND REMARKS

Macroscopic magnetic systems subjected to external forcing exhibit self-organization phenomena as a result of

injection, transport, and dissipation of energy and momenta. For extended systems, natural self-organization states are spatial structures. In this work, we have studied the formation of spatial patterns from a uniform magnetization state in one and two spatial dimensions in a spin-transfer nano-oscillator induced by the competition of a spin-polarized current and an external magnetic field. This system is described in the continuous limit by the Landau-Lifshitz-Gilbert equation. This model incorporates the uniaxial anisotropy, the demagnetization in thin film approximation, the ferromagnetic exchange that provides the spatial coupling, the dissipation, and a spin-transfer torque term. The bifurcation diagram of the parallel state to external magnetic field is revealed. It is important to note that the bifurcation diagram of the antiparallel state is similar to that exhibited by the parallel state, since the parallel state is related with the antiparallel one through the transformation $(g,h_a,\varphi) \to (-g, -h_a,\varphi + \pi)$.

We have shown analytically that the parallel state has a spatial supercritical quintic bifurcation. Numerical simulations at the onset of spatial bifurcation verify these theoretical results. In addition, we have determined that there is a critical value for the external magnetic field, h_a^c, in which the transition becomes seventh type. For $|h_a| < |h_a^c|$, the dominant mechanism that makes the pattern saturate is the anisotropy, however for $|h_a| > |h_a^c|$, the mechanism that drives the dynamics is the ferromagnetic exchange. In two spatial dimensions the system shows the emergence of stripe patterns or superlattices at the onset of bifurcations. Analytically, we have characterized its respective bifurcation diagram, which is characterized by a single control parameter, which accounts for the competition between the external magnetic field, anisotropy, exchange, and the critical spin-polarized current. This scenario is confirmed numerically. Therefore, when the anisotropy is the dominant mechanism ($|h_a| < |h_a^c|$) the system exhibits striped patterns, however, in the case of the exchange driving the dynamics ($|h_a| > |h_a^c|$), the system presents superlattice as stable equilibria. Indeed, exchange favors the formation of more complicated structures.

For typical experimental setups, the anisotropies are about $\beta_x = 0.5$ and $\beta_z = 1$, and the exchange length is of the order of 3.5 nm. Then for external fields of magnitude $H_a = M_s|h_a| = 1.5M_s$, the wavelength of the pattern is typically of order $\Lambda = 30$ nm. One expects that self-organization exhibited in this study persists for generalizations or variations of model (2). For instance, the angular dependence of g [18,27–32] or the use tensor form of magnetization damping [43] could change the saturation mechanisms of patterns for some geometries and materials, due to the inclusion of other terms. Work in this direction is in progress.

ACKNOWLEDGMENTS

We thank N. Perinet for useful discussions. The authors acknowledge the financial support by ANR-CONICYT 39 (ANR-2010-INTB-402-02), "Colors". M.G.C. thanks the financial support of FONDECYT Project No. 1120320. A.O.L. thanks CONICYT fellowship Beca Nacional, Contract No. 21120878, and ANR-CONICYT 39 (ANR-2010-INTB-402-02) for supporting a collaboration visit at Université des Sciences et Technologies de Lille.

[1] G. Nicolis and I. Prigogine, *Self-Organization in Non Equilibrium Systems* (Wiley, New York, 1977).
[2] L. M. Pismen, *Patterns and Interfaces in Dissipative Dynamics* (Springer, Berlin, 2006).
[3] M. C. Cross and P. C. Hohenberg, Rev. Mod. Phys. **65**, 851 (1993).
[4] M. Cross and H. Greenside, *Pattern Formation and Dynamics in Nonequilibrium Systems* (Cambridge University Press, New York, 2009).
[5] M. I. Rabinovich, A. B. Ezersky, and P. D. Weidman, *The Dynamics of Patterns* (World Scientic, Singapore, 2000).
[6] G. Nicolis, *Introduction to Nonlinear Science* (Cambridge University Press, Cambridge, 1995).
[7] P. Ball, *The Self-Made Tapestry: Pattern Formation in Nature* (Oxford University Press, New York, 1999).
[8] R. B. Hoyle, *Pattern Formation: An Introduction to Methods* (Cambridge University Press, Cambridge, 2006).
[9] A. C. Newell, T. Passot, and J. Lega, Ann. Rev. Fluid Mech. **25**, 399 (1993).
[10] I. Ortega, M. G. Clerc, C. Falcon, and N. Mujica, Phys. Rev. E **81**, 046208 (2010).
[11] L. Landau, C. R. Acad. Sci. USSR **44**, 311 (1944).
[12] W. S. Edwards and S. Fauve, Phys. Rev. E **47**, R788 (1993).
[13] E. Pampaloni, P. L. Ramazza, S. Residori, and F. T. Arecchi, Phys. Rev. Lett. **74**, 258 (1995).
[14] M. Le Berre, E. Ressayre, A. Tallet, Y. Pomeau, and L. Di Menza, Phys. Rev. E **66**, 026203 (2002).
[15] B. Georges, J. Grollier, M. Darques, V. Cros, C. Deranlot, B. Marcilhac, G. Faini, and A. Fert, Phys. Rev. Lett. **101**, 017201 (2008).
[16] Z. Yang, S. Zhang, and Y. C. Li, Phys. Rev. Lett. **99**, 134101 (2007).
[17] D. Li, Y. Zhou, C. Zhou, and B. Hu, Phys. Rev. B **83**, 174424 (2011); and references therein.
[18] J. C. Slonczewski, J. Magn. Magn. Mater. **159**, L1 (1996).
[19] L. Berger, Phys. Rev. B **54**, 9353 (1996).
[20] S. I. Kiselev, J. C. Sankey, I. N. Krivorotov, N. C. Emley, R. J. Schoelkopf, R. A. Buhrman, and D. C. Ralph, Nature (London) **425**, 380 (2003).
[21] D. C. Ralph and M. D. Stiles, J. Magn. Magn. Mater. **320**, 1190 (2008).
[22] G. Bertotti, C. Serpico, I. D. Mayergoyz, A. Magni, M. d'Aquino, and R. Bonin, Phys. Rev. Lett. **94**, 127206 (2005).
[23] R. Bonin, M. d'Aquino, G. Bertotti, C. Serpico, and I. D. Mayergoyz, Eur. Phys. J. B **85**, 47 (2012).
[24] I. D. Mayergoyz, G. Bertotti, and C. Serpico, *Nonlinear Magnetization Dynamics in Nanosystems* (Elsevier, Oxford, 2009).
[25] Z. Li and S. Zhang, Phys. Rev. B **68**, 024404 (2003); J. Z. Sun, *ibid.* **62**, 570 (2000); X. Waintal, E. B. Myers, P. W. Brouwer,

and D. C. Ralph, *ibid.* **62**, 12317 (2000); M. D. Stiles and A. Zangwill, *ibid.* **66**, 014407 (2002).
[26] G. Gioia and R. D. James, Proc. R. Soc. Lond. A **453**, 213 (1997).
[27] J. C. Slonczewski, J. Magn. Magn. Mater. **247**, 324 (2002).
[28] J. Xiao, A. Zangwill, and M. D. Stiles, Phys. Rev. B **70**, 172405 (2004).
[29] J. Xiao, A. Zangwill, and M. D. Stiles, Phys. Rev. B **72**, 014446 (2005).
[30] J. Barnas, A. Fert, M. Gmitra, I. Weymann, and V. K. Dugaev, Phys. Rev. B **72**, 024426 (2005).
[31] S.-W. Lee and K.-J. Lee, IEEE Trans. Magn. **46**, 2349 (2010).
[32] W. Kim, S.-W. Lee, and K.-J. Lee, J. Phys. D **44**, 384001 (2011).
[33] M. Lakshmanan, Phil. Trans. R. Soc. A **369**, 1280 (2011).
[34] E. Atlee Jackson, *Perspectives of Nonlinear Dynamics* (Cambridge University Press, New York, 1989), Vol. 1.
[35] Y. Kuznetsov, *Elements of Applied Bifurcation Theory*, 2nd ed. (Springer, New York, 2004).
[36] R. M. Hornreich and M. Luban, Phys. Rev. Lett. **35**, 1678 (1975).
[37] P. Glansdorff and I. Prigogine, *Thermodynamic Theory of Structure, Stability, and Fluctuations* (Wiley, New York, 1974).
[38] A. De Wit, D. Lima, G. Dewel, and P. Borckmans, Phys. Rev. E **54**, 261 (1996).
[39] P. Coullet, T. Frisch, and G. Sonnino, Phys. Rev. E **49**, 2087 (1994).
[40] G. Agez, M. G. Clerc, E. Louvergneaux, and R. G. Rojas, Phys. Rev. E **87**, 042919 (2013).
[41] F. Petrelis, S. Aumaitre, and S. Fauve, Phys. Rev. Lett. **94**, 070603 (2005).
[42] B. A. Malomed, A. A. Nepomnyashchy, and M. I. Tribelsky, Phys. Rev. A **42**, 7244 (1990).
[43] V. L. Safonov, J. Appl. Phys. **91**, 8653 (2002).